Electronic Supplementary Material (ESI) for Inorganic Chemistry Frontiers.

Electronic Supplementary Information for

Generation and nature of water-tolerant Lewis acid sites in $In_xSn_{10-x}O_y/Al_2O_3$ catalyst as active centers for green synthesis of methyl lactate from glucose

Zhenxiang Zhao[a], Jun Yang[a], Ningkun Xu[a], Tian Nan[a], Pingping Wu[a], Chunzheng Wang[a], Xiaohua Wang[b], Peng Bai[a,], Zifeng Yan[a] and Svetlana Mintova[a,c]*

[a] State Key Laboratory of Heavy Oil Processing, CNPC Key Laboratory of Catalysis, College of Chemistry and Chemical Engineering, China University of Petroleum (East China), Qingdao 266580, China

[b] Petrochemical Research Institute, PetroChina Company Limited, Beijing 100195, China

[c] Normandie University, ENSICAEN, UNICAEN, CNRS, Laboratoire Catalyse et Spectrochimie, 14000 Caen, France

* Corresponding authors. Tel: +86-532-86981812;

*E-mail address:*baipeng@upc.edu.cn *(P. Bai)*

Table S1. Preparation details of catalysts.

Sample name	M/Al [a]	In/Sn [b]	Metal precursor	Solvent
In/Al_2O_3	0.1	-	$In(NO_3)_3$	ethanol
$In_9Sn_1O_y/Al_2O_3$	0.1	9/1	$In(NO_3)_3+SnCl_2 \cdot 2H_2O$	ethanol
$In_8Sn_2O_y/Al_2O_3$	0.1	8/2	$In(NO_3)_3+SnCl_2 \cdot 2H_2O$	ethanol
$In_7Sn_3O_y/Al_2O_3$	0.1	7/3	$In(NO_3)_3+SnCl_2 \cdot 2H_2O$	ethanol
Sn_{II}/Al_2O_3	0.1	0	$SnCl_2 \cdot 2H_2O$	ethanol
Sn_{IV}/Al_2O_3	0.1	-	$SnCl_4$	H_2O

[a] The molar ratio of active metal to Al (M are the metals); [b] The molar ratio of In to Sn.

Table S2. Textural properties of catalysts.

Sample name	S_{BET} ($m^2 \cdot g^{-1}$)	Pore size (nm)	Pore volume ($cm^3 \cdot g^{-1}$)
Al_2O_3	246.7±5.6	12.3±0.1	1.03±0.03
In/Al_2O_3	199.6±2.4	12.3±0.1	0.78±0.04
$In_9Sn_1O_y/Al_2O_3$	188.2±3.2	12.2±0.2	0.73±0.03
$In_7Sn_3O_y/Al_2O_3$	194.1±4.3	12.3±0.2	0.52±0.05
$In_5Sn_5O_y/Al_2O_3$	190.9±5.5	12.3±0.3	0.67±0.02
Sn_{II}/Al_2O_3	185.4±6.5	12.3±0.2	0.69±0.03

Table S3. Weight loss of catalysts at different temperatures after adsorption of glucose or after the reaction.[a]

	Weight loss of catalyst (%)[b]	Weight loss of catalyst after adsorption (%)[c]	Residual organics (%)[d]
Al_2O_3	2.39	5.12	20.30±0.34
Sn_{IV}/Al_2O_3	2.73	3.38	13.79±0.45
In/Al_2O_3	2.38	2.82	7.48±0.44
$In_9Sn_1O_y/Al_2O_3$	2.76	3.58	5.67±0.45
$In_7Sn_3O_y/Al_2O_3$	3.05	2.30	6.74±0.51
$In_5Sn_5O_y/Al_2O_3$	2.60	3.38	9.12±0.45
Sn_{II}/Al_2O_3	3.16	0.26	5.72±0.32

[a]:all data based on TGA analysis; [b] mass of catalyst (100 °C)- mass of catalyst (800 °C); [c]:mass of catalyst after adsorption (100 °C)- mass of catalyst after adsorption (800 °C)- weight loss of catalyst; [d] mass of catalyst after reaction (100 °C)- mass of catalyst after reaction (800 °C)- weight loss of catalyst.

Table S4. Reaction conditions and MLA yields of catalyst reported earlier.

Catalyst	Temperature (°C)	Time (h)	MLA Yield (%)	Ref.
NaOH+[IMEP]Cl	100	0.5	63	1
KOH+[IMEP]Cl	100	0.5	65.5	1
NH_4OH+[IMEP]Cl	100	0.5	7	1
$Ca(OH)_2$+[IMEP]Cl	100	0.5	21	1
$Ba(OH)_2$+[IMEP]Cl	100	0.5	26	1
NaOH+[IMEP]BF_4	100	0.5	58.1	1
NaOH+[IMEP]ClO_4	100	0.5	50.1	1
NaOH+[IMEP]Ac	100	0.5	44.8	1
NaOH+[IMEP]PF_6	100	0.5	9.5	1
NaOH+[IMEP]PhCOO	100	0.5	33.2	1
$Co(NO_3)_2$	200	1	14.3	2
$Ba(OH)_2$	25	48	95.4	3
Sn-BEA	160	20	43	4
Sn-BEA	160	16	52	5
Sn-BEA	160	10	45	6
Sn-BEA	160	8	>55	7
Sn-BEA	160	20	52.5	8
Sn-BEA	160	10	58	9
Al_2O_3	160	6	34	10

ZrO_2	160	6	6	10
TiO_2	160	6	10	10
CeO_2	160	6	14	10
Al_2O_3	180	5	21	11
In_2O_3	180	12	14	11
In/Al_2O_3	180	12	42	11
$In/Al_2O_3+K_2CO_3$	180	12	49	11
La_2O_3	200	1	18.8	2
Co_2O_3	200	1	31.3	2
$LaCoO_3$	200	1	39.5	2
SnO_2	160	6	1	10
Al_2O_3	160	10	25.9±1.6	This work
In/Al_2O_3	160	10	47.8±1.3	This work
$In_9Sn_1O_y/Al_2O_3$	160	10	31.9±1.3	This work
$In_7Sn_3O_y/Al_2O_3$	160	10	57.6±1.2	This work
$In_5Sn_5O_y/Al_2O_3$	160	10	41.3±1.0	This work
Sn_{II}/Al_2O_3	160	10	19.2±1.2	This work
Sn_{IV}/Al_2O_3	160	10	28.3±1.1	This work

Table S5. Regeneration-reaction cycle stability of catalysts.

Entry	Catalyst	MLA yield	Ref.
1	$In_7Sn_3O_y/Al_2O_3$ [a]	57.6 %±1.2 %	This work
2	$In_7Sn_3O_y/Al_2O_3$ [b]	59.4 %±1.8 %	This work

3	$In_7Sn_3O_y/Al_2O_3$ [c]	53.0 %±1.3 %	This work
4	Al_2O_3 [a]	25.9 %±1.6 %	This work
5	Al_2O_3 [b]	6.5 %±1.5 %	This work
6	Al_2O_3 [a]	34 %	[10]
7	Al_2O_3 [b]	25 %	[10]
8	Al_2O_3 [c]	21 %	[10]

a 1st use; *b* 2nd use; *c* 3rd use;

Table S6. Amount of LAS of catalysts measured by NH_3-TPD.

Sample name	Acid (μmol/g) [a]
$In_7Sn_3O_y/Al_2O_3$	269.47±13
In/Al_2O_3	363.59±14

a The acid amount was calculated based on the measure results of NH_3-TPD.

Table S7. Adsorption energies calculated for samples $In_7Sn_3O_y$ and In_2O_3.

	$E_{surface}$ (Ha)	$E_{adsorbate}$ (Ha)	$E_{adsorbate/surface}$ (Ha)	E_{ads} (Ha)	E_{ads} (eV)	E_{ads} (kcal/mol)
$In_7Sn_3O_y$	-16788.058	-686.691	-17474.7491	-0.05385	-1.46542	-33.8
In_2O_3	-16630.992	-686.691	-17317.68307	-0.03086	-0.83988	-19.4

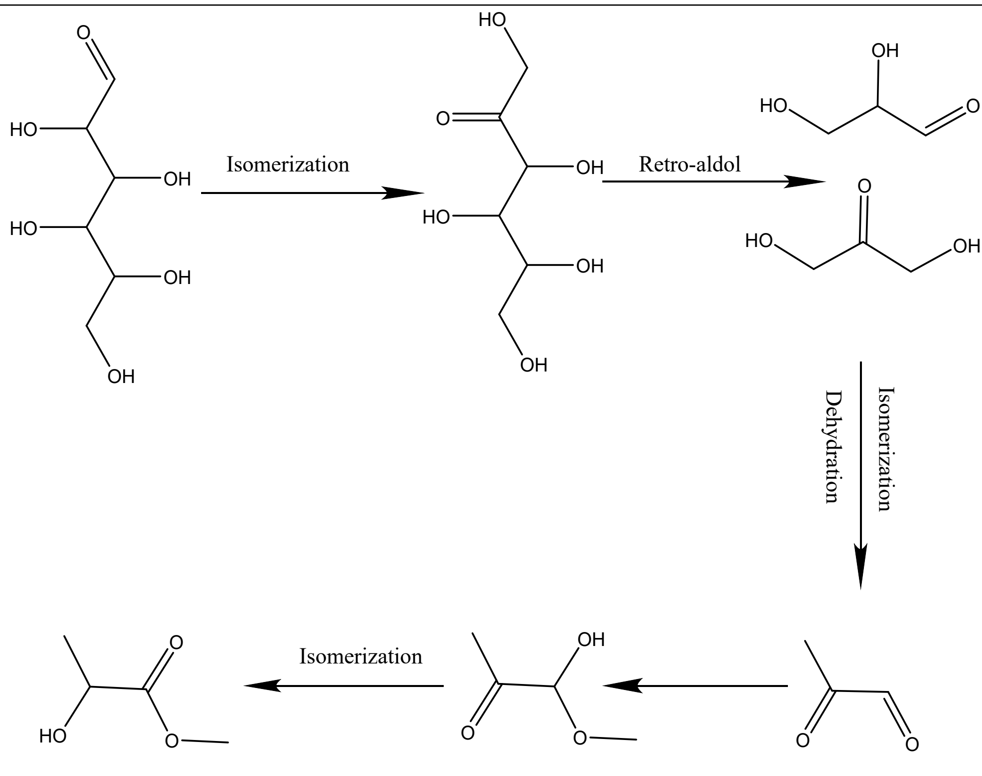

Fig. S1 The conversion process of glucose to MLA.

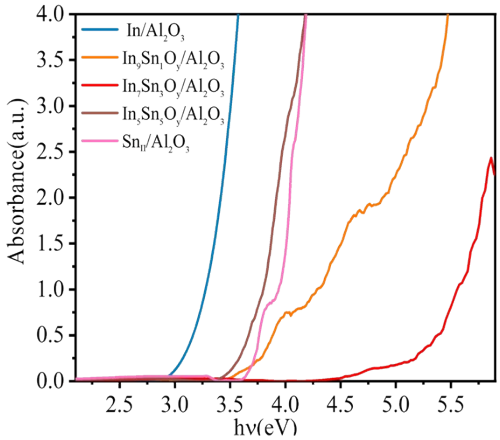

Fig. S2 Band gap analysis of In/Al_2O_3, $In_9Sn_1O_y/Al_2O_3$, $In_7Sn_3O_y/Al_2O_3$, $In_5Sn_5O_y/Al_2O_3$, Sn_{II}/Al_2O_3 catalysts.

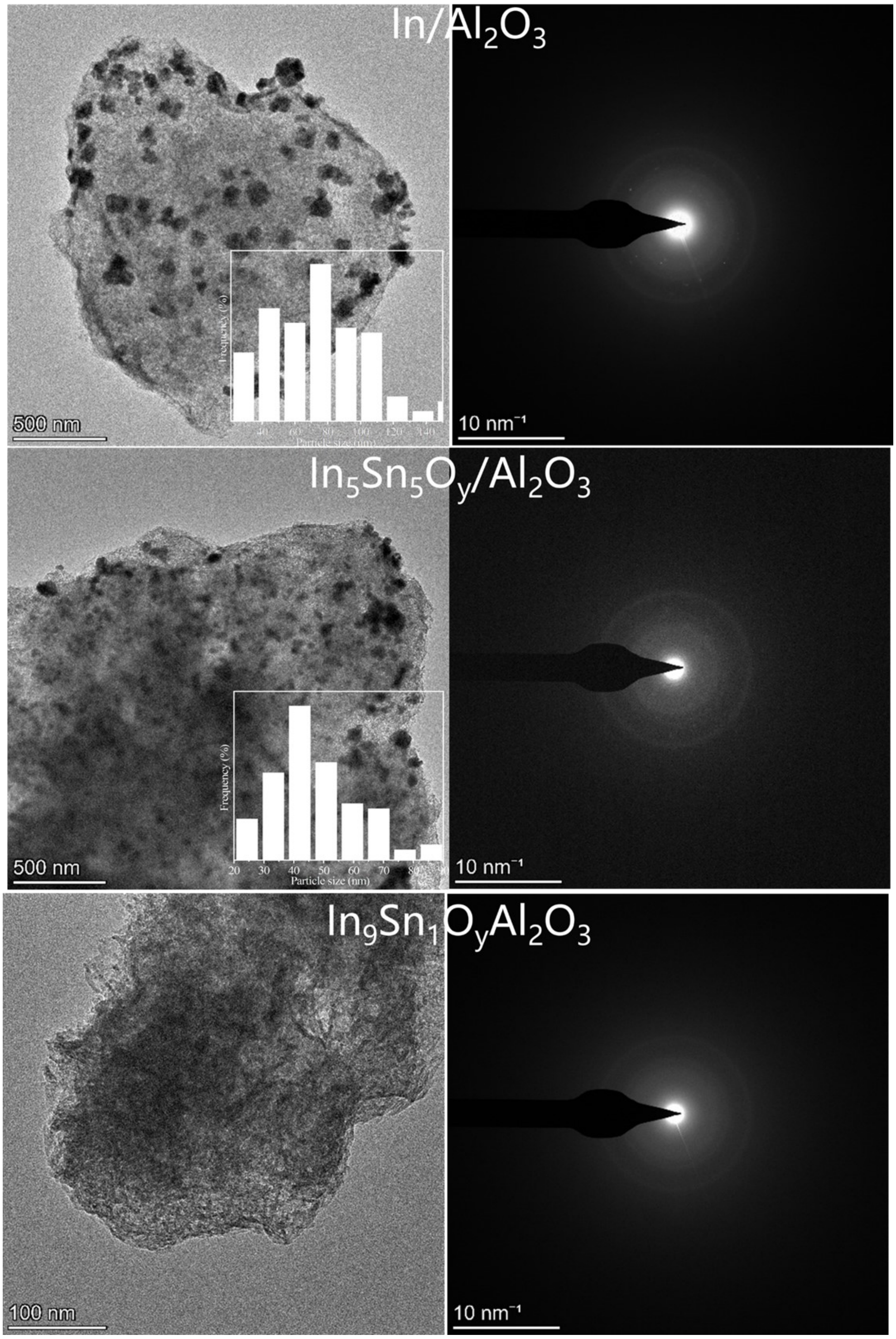

Fig. S3 TEM images of In/Al_2O_3, $In_9Sn_1O_y/Al_2O_3$, $In_5Sn_5O_y/Al_2O_3$ catalysts. Insets show the particle size distribution diagrams.

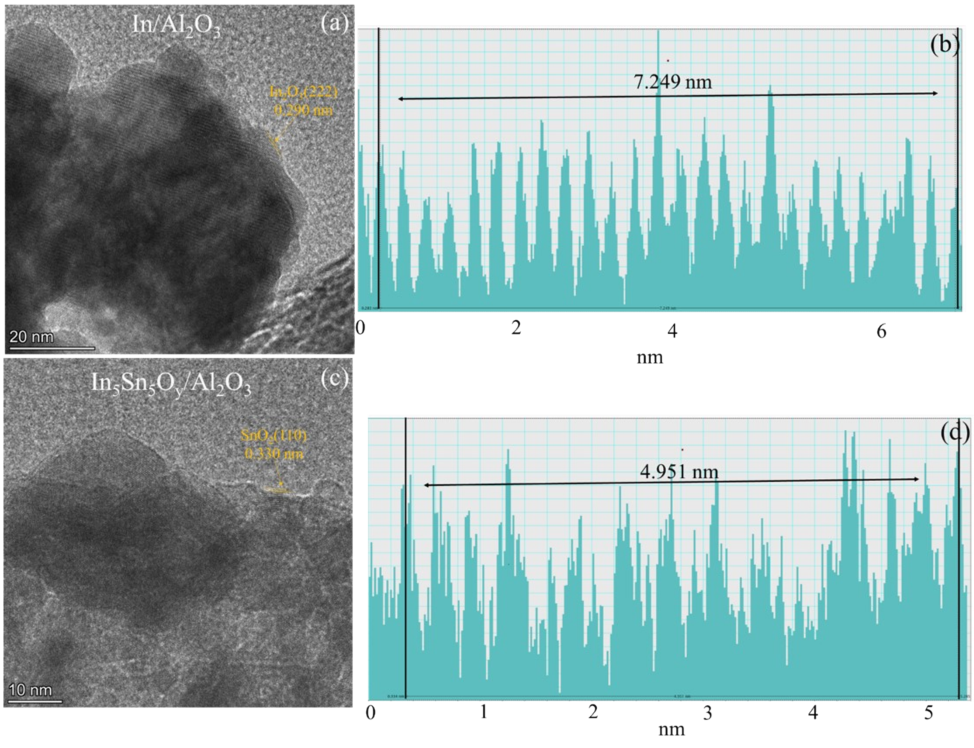

Fig. S4 HRTEM images of In/Al_2O_3(a), $In_5Sn_5O_y/Al_2O_3$ (c) and lattice spacings of In/Al_2O_3 (b), $In_5Sn_5O_y/Al_2O_3$ (d).

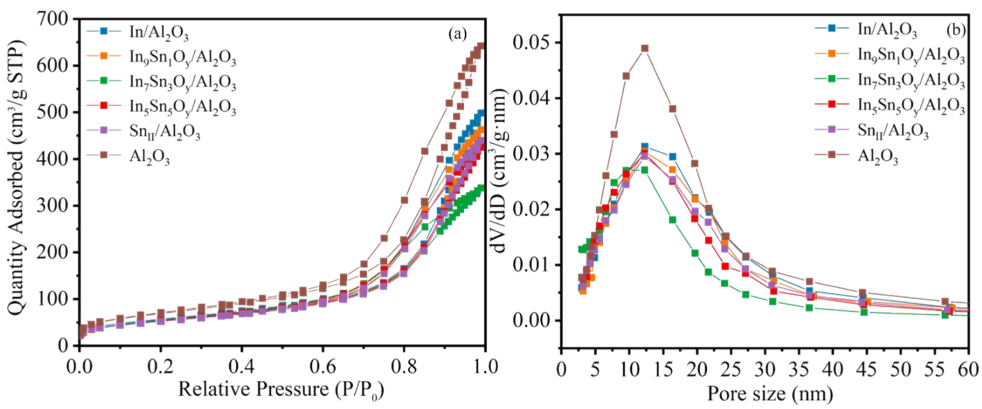

Fig. S5 Nitrogen adsorption and desorption isotherms (a) and pore size distribution curves (b) of In/Al_2O_3, $In_9Sn_1O_y/Al_2O_3$, $In_7Sn_3O_y/Al_2O_3$, $In_5Sn_5O_y/Al_2O_3$, Sn_{II}/Al_2O_3 catalysts.

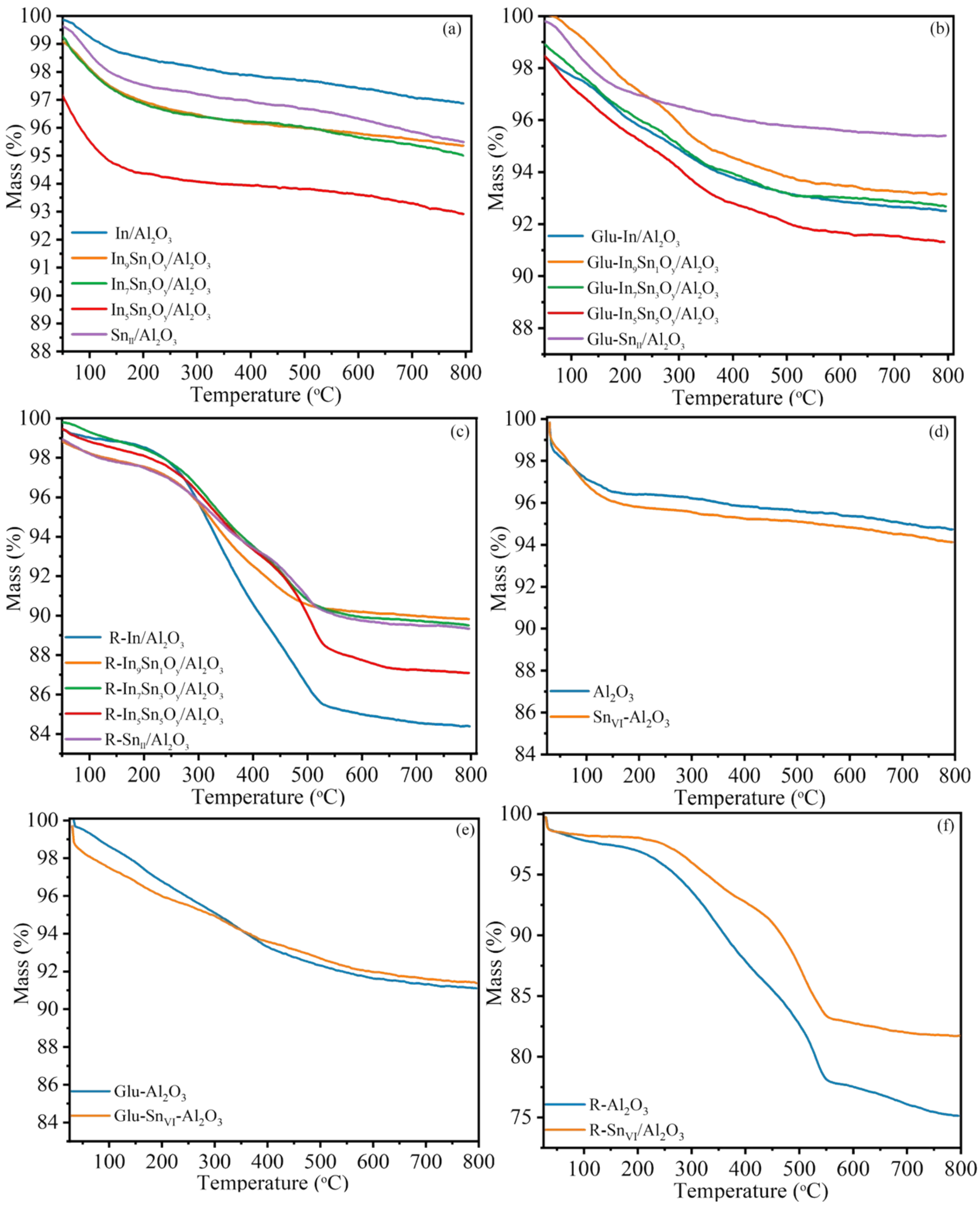

Fig. S6 TG curves of $In_xSn_{10-x}O_y/Al_2O_3$ (a), $In_xSn_{10-x}O_y/Al_2O_3$ after glucose adsorption (b), $In_xSn_{10-x}O_y/Al_2O_3$ after reaction (c); TG curves of M/Al_2O_3 (d), M/Al_2O_3 after glucose adsorption (e), M/Al_2O_3 after reaction (f).

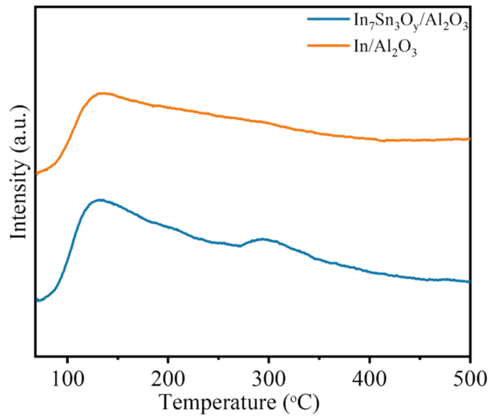

Fig. S7 NH_3-TPD profiles of $In_7Sn_3O_y/Al_2O_3$, In/Al_2O_3 catalysts.

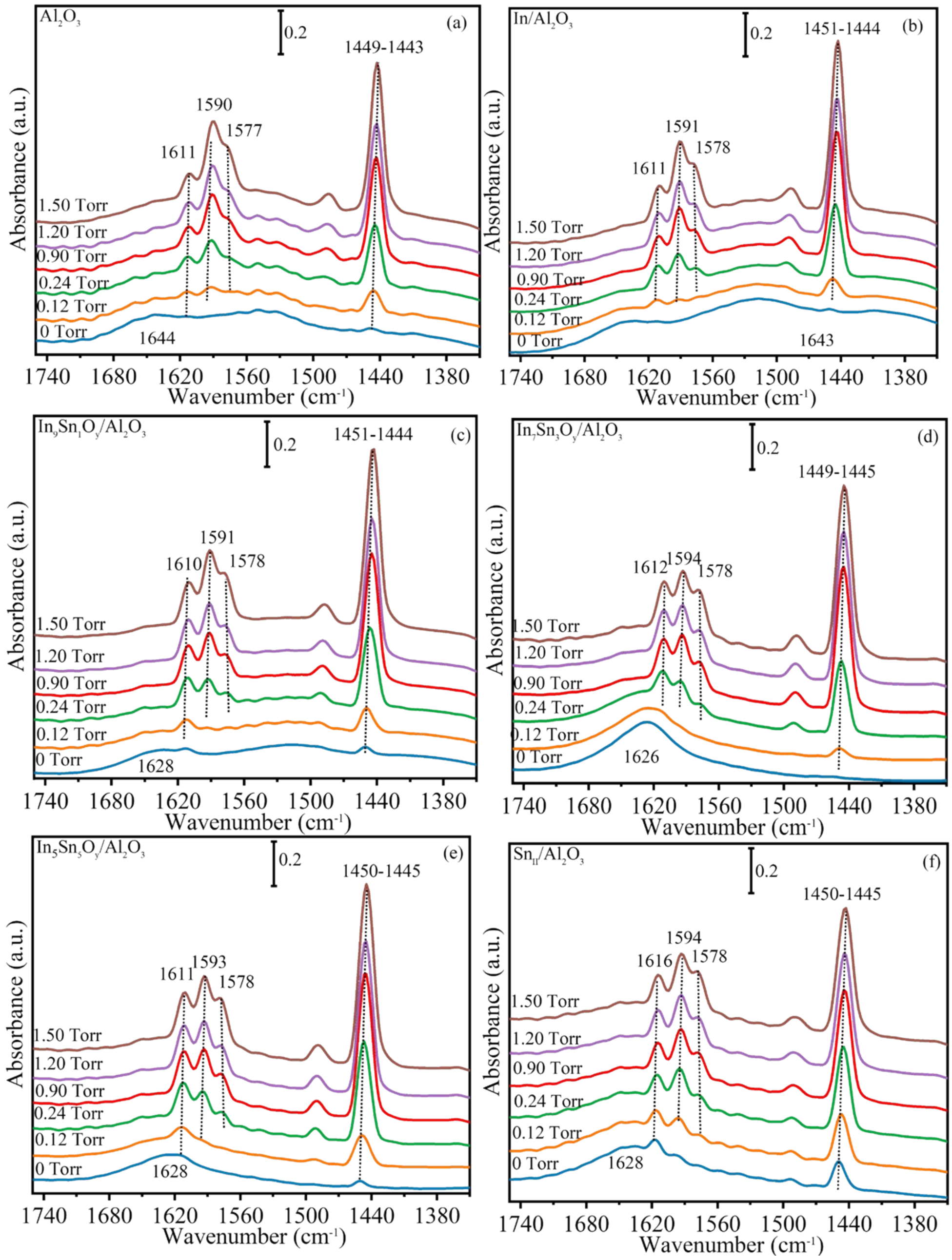

Fig. S8 FT-IR spectra of competitive adsorption of pyridine and water on Al_2O_3, In/Al_2O_3, $In_9Sn_1O_y/Al_2O_3$, $In_7Sn_3O_y/Al_2O_3$, $In_5Sn_5O_y/Al_2O_3$, Sn_{II}/Al_2O_3 catalysts.

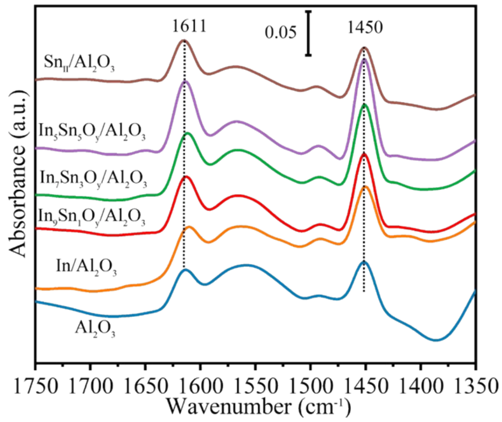

Fig. S9 Py-FT-IR spectra of Al_2O_3, In/Al_2O_3, $In_9Sn_1O_y/Al_2O_3$, $In_7Sn_3O_y/Al_2O_3$, $In_5Sn_5O_y/Al_2O_3$, Sn_{II}/Al_2O_3 catalysts.

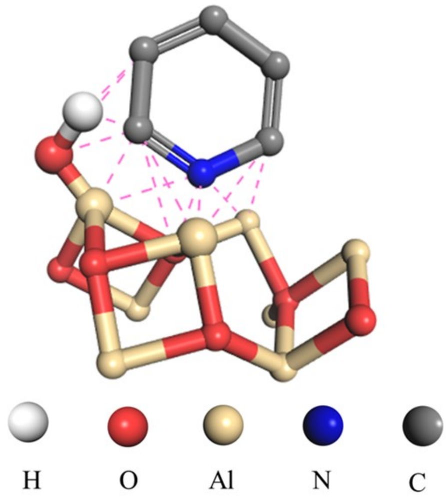

Fig. S10 pyridine adsorbed on LAS of Al_2O_3.[12]

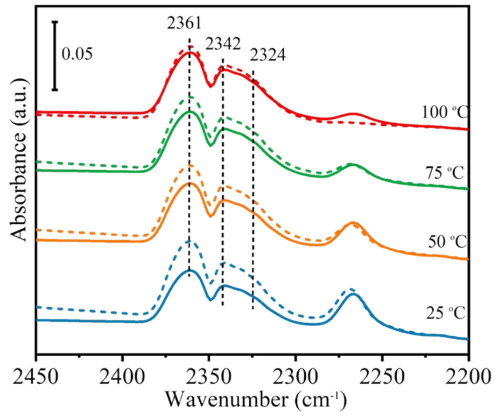

Fig. S11 IR spectra of $In_7Sn_3O_y/Al_2O_3$ using CD_3CN probe molecule with and without water after desorption at different temperatures. (The spectra have been normalized according to the sample mass. Solid line: pure CD_3CN adsorption; Dotted line: CD_3CN co-adsorption with water)

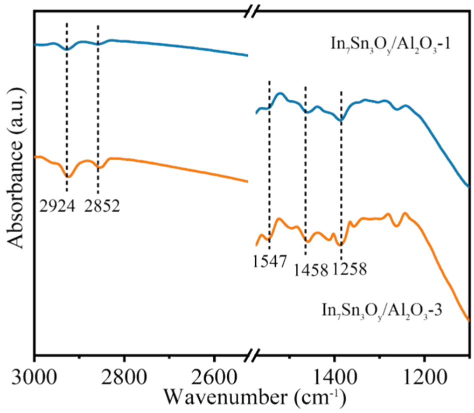

Fig. S12 FT-IR spectra of catalysts after reaction: $In_7Sn_3O_y/Al_2O_3$-x (x: reaction-regeneration cycles times).

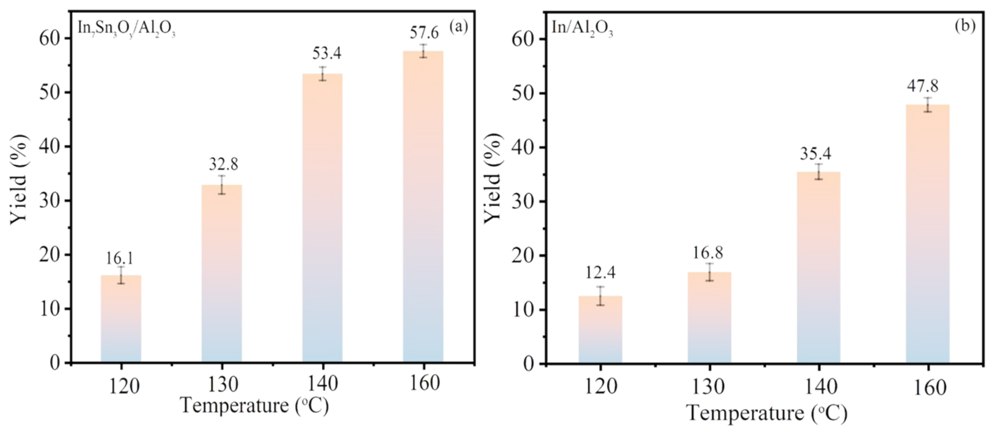

Fig. S13 MLA yield on $In_7Sn_3O_y/Al_2O_3$ (a) and In/Al_2O_3 (b) catalysts.

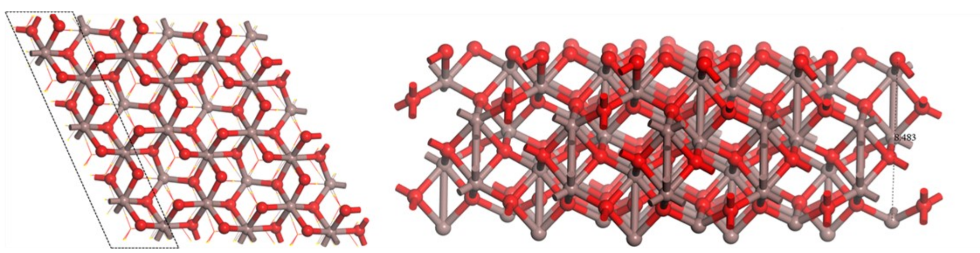

Fig. S14 Models of In_2O_3(222).

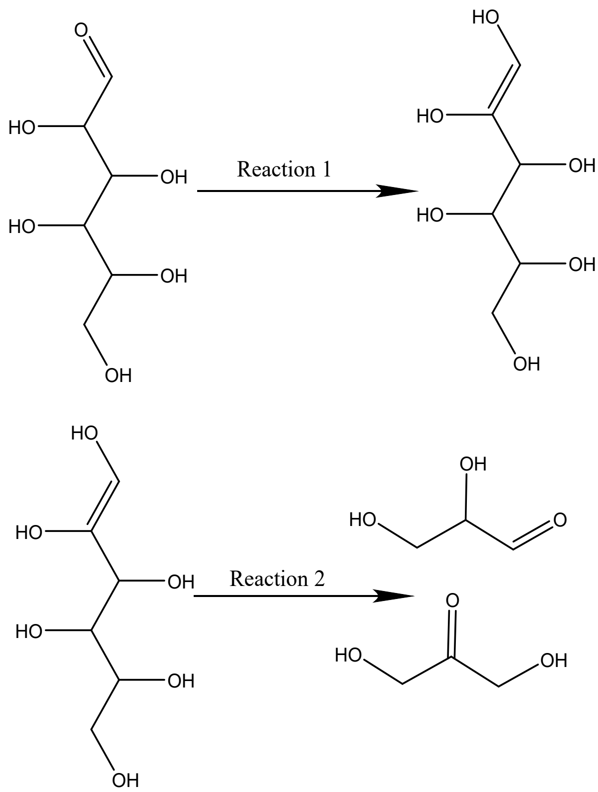

Fig. S15 The reaction pathway for DFT calculations (Reaction 1: Conversion of glucose to enol; Reaction 2: Conversion of enol to glyceraldehyde and dihydroxy acetone;).

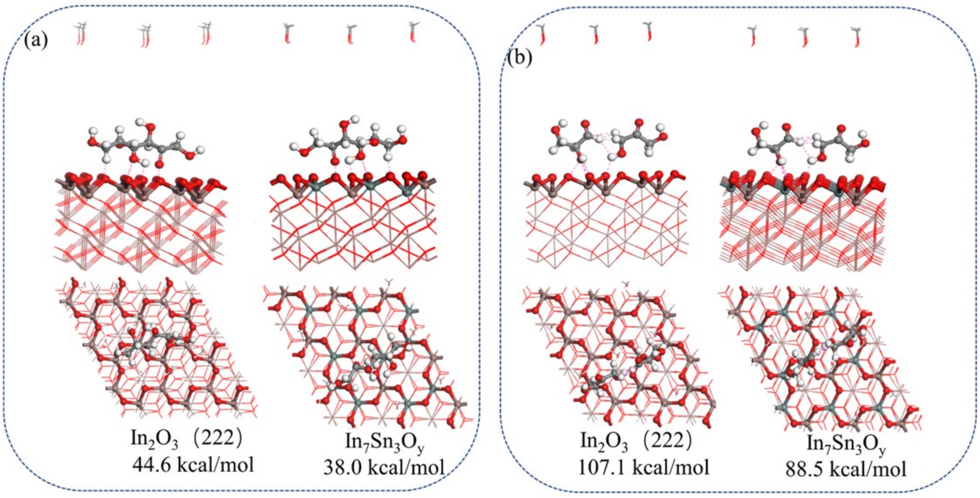

Fig. S16 (a) Energies of glucose forming enol on the In_2O_3 (222) and $In_3Sn_7O_y$ (kcal/mol), (b) energies of enol to glyceraldehyde and dihydroxy acetone on the In_2O_3 (222) and In_3Sn_7Oy models (kcal/mol). (Color code: red is O, white is H, gray is C, brown is In, and cyan is Sn.).

References

1. X. Wang, Y. Song, C. Huang, F. Liang and B. Chen, Lactic Acid Production from Glucose over

Polymer Catalysts in Aqueous Alkaline Solution under Mild Conditions, *Green Chem.*, 2014, **16**, 4234-4240.
2. X. Yang, L. Yang, W. Fan and H. Lin, Effect of Redox Properties of LaCoO3 Perovskite Catalyst on Production of Lactic Acid from Cellulosic Biomass, *Catal. Today*, 2016, **269**, 56-64.
3. L. Li, F. Shen, R. L. Smith and X. Qi, Quantitative Chemocatalytic Production of Lactic Acid from Glucose under Anaerobic Conditions at Room Temperature, *Green Chem.*, 2017, **19**, 76-81.
4. M. S. Holm, S. Saravanamurugan and E. Taarning, Conversion of Sugars to Lactic Acid Derivatives Using Heterogeneous Zeotype Catalysts, *Science*, 2010, **328**, 602-605.
5. M. S. Holm, Y. J. Pagán-Torres, S. Saravanamurugan, A. Riisager, J. A. Dumesic and E. Taarning, Sn-Beta Catalysed Conversion of Hemicellulosic Sugars, *Green Chem.*, 2012, **14**, 702-706.
6. X. Yang, Y. Liu, X. Li, J. Ren, L. Zhou, T. Lu and Y. Su, Synthesis of Sn-Containing Nanosized Beta Zeolite As Efficient Catalyst for Transformation of Glucose to Methyl Lactate, *ACS Sustain. Chem. Eng.*, 2018, **6**, 8256-8265.
7. B. Tang, S. Li, W.-C. Song, E.-C. Yang, X.-J. Zhao, N. Guan and L. Li, Fabrication of Hierarchical Sn-Beta Zeolite as Efficient Catalyst for Conversion of Cellulosic Sugar to Methyl Lactate, *ACS Sustain. Chem. Eng.*, 2020, **8**, 3796-3808.
8. J. Zhang, L. Wang, G. Wang, F. Chen, J. Zhu, C. Wang, C. Bian, S. Pan and F.-S. Xiao, Hierarchical Sn-Beta Zeolite Catalyst for the Conversion of Sugars to Alkyl Lactates, *ACS Sustain. Chem. Eng.*, 2017, **5**, 3123-3131.
9. X. Yang, J. Bian, J. Huang, W. Xin, T. Lu, C. Chen, Y. Su, L. Zhou, F. Wang and J. Xu, Fluoride-free and Low Concentration Template Synthesis of Hierarchical Sn-Beta Zeolites: Efficient Catalysts for Conversion of Glucose to Alkyl Lactate, *Green Chem.*, 2017, **19**, 692-701.
10. S. Yamaguchi, M. Yabushita, M. Kim, J. Hirayama, K. Motokura, A. Fukuoka and K. Nakajima, Catalytic Conversion of Biomass-Derived Carbohydrates to Methyl Lactate by Acid–Base Bifunctional γ-Al_2O_3, *ACS Sustain. Chem. Eng.*, 2018, **6**, 8113-8117.
11. Y. Xiao, S. Xu, W. Zhang, J. Li and C. Hu, One-pot Chemo-catalytic Conversion of Glucose to Methyl Lactate over In/γ-Al_2O_3 Catalyst, *Catal. Today*, 2021, **365**, 249-256.
12. Liu and Xinsheng, DRIFTS Study of Surface of γ-Alumina and Its Dehydroxylation, *J. Phys. Chem. C*, 2008, **112**, 5066-5073.

Abbreviation Index:

methyl lactate:MLA
Lewis acid sites:LAS
coordinatively unsaturated sites:CUS
polylactic acid:PLA
lactic acid:LA
zeolite Beta:BEA
dealumination of BEA zeolite:deAl-BEA
In-Sn oxide:ITO
pyridine:Py
acetonitrile-d3:CD_3CN
ultraviolet-visible:UV-vis
Transmission electron microscopy:TEM
selected area electron diffraction:SAED
Scanning transmission electron microscope-high angle annular dark field:STEM-HAADF
X-ray energy dispersive spectroscopy:EDS
Barret-Joyner-Halenda:BJH
X-ray photoelectron spectra:XPS
binding energies:BE
thermogravimetric analysis:TGA

Density Functional Theory:DFT
generalized gradient approximation:GGA
Perdew Burke Ernzerhof:PBE
gas chromatograph:GC
flame ionization detector:FID
tin containing zeolite Beta:Sn-BEA
glyceraldehyde:GLY
dihydroxyacetone:DHA
tetrahedrally-coordinated M^{n+}: (M^{IV})
octahedrally-coordinated M^{n+}: (M^{VI})
penta-coordinated M^{n+}: (M^{V})